Sputter deposition of $Mg_xAl_yO_z$ thin films in a dual-magnetron device: a multi-species Monte Carlo model

2012 New J. Phys. 14 073043

(http://iopscience.iop.org/1367-2630/14/7/073043)

New Journal of Physics
The open-access journal for physics

Sputter deposition of $Mg_xAl_yO_z$ thin films in a dual-magnetron device: a multi-species Monte Carlo model

M Yusupov[1,3], M Saraiva[2], D Depla[2] and A Bogaerts[1]

[1] Research Group PLASMANT, Department of Chemistry, University of Antwerp, Universiteitsplein 1, 2610 Antwerp, Belgium
[2] Research Group DRAFT, Department of Solid State Sciences, Ghent University, Krijgslaan 281 (S1), B-9000 Ghent, Belgium
E-mail: maksudbek.yusupov@ua.ac.be

New Journal of Physics **14** (2012) 073043 (21pp)
Received 20 July 2011
Published 20 July 2012
Online at http://www.njp.org/
doi:10.1088/1367-2630/14/7/073043

Abstract. A multi-species Monte Carlo (MC) model, combined with an analytical surface model, has been developed in order to investigate the general plasma processes occurring during the sputter deposition of complex oxide films in a dual-magnetron sputter deposition system. The important plasma species, such as electrons, Ar^+ ions, fast Ar atoms and sputtered metal atoms (i.e. Mg and Al atoms) are described with the so-called multi-species MC model, whereas the deposition of $Mg_xAl_yO_z$ films is treated by an analytical surface model. Target–substrate distances for both magnetrons in the dual-magnetron setup are varied for the purpose of growing stoichiometric complex oxide thin films. The metal atoms are sputtered from pure metallic targets, whereas the oxygen flux is only directed toward the substrate and is high enough to obtain fully oxidized thin films but low enough to avoid target poisoning. The calculations correspond to typical experimental conditions applied to grow these complex oxide films. In this paper, some calculation results are shown, such as the densities of various plasma species, their fluxes toward the targets and substrate, the deposition rates, as well as the film stoichiometry. Moreover, some results of the combined model are compared with experimental observations. Note that this is the first complete model, which can be applied for large and complicated magnetron reactor geometries, such as dual-magnetron configurations. With this model,

[3] Author to whom any correspondence should be addressed.

we are able to describe all important plasma species as well as the deposition process. It can also be used to predict film stoichiometries of complex oxide films on the substrate.

Contents

1. Introduction

The deposition of thin films plays a central role in many key technologies, including the fabrication of anti-reflective, hard and wear-resistant materials, computer hard drives and high-performance optical coatings. Magnetron sputtering is the most widely used method for the deposition of various types of industrially important coatings, such as metals, oxides and nitrides [1].

Besides an electric field, a magnetic field is also present in a magnetron discharge, which can cause the electrons to be trapped in an area close to the cathode. This gives rise to a more effective use of the electrons for ionization of the background gas atoms, which results in enhanced sputtering of the target in comparison with a non-magnetized discharge. Because of this efficient ionization, magnetrons can operate at lower pressures (typically in the range of 0.1–1 Pa [2]). Due to the lower pressure, the sputtered atoms are less scattered on their way to the substrate, which results in a more effective deposition.

Magnetron discharges with two (or more) sources are now widely used in the sputter deposition of complex oxide films (e.g. $Mg_xAl_yO_z$). There exist different configurations of magnetrons with two sources (or so-called dual magnetrons), and each of them has its specific advantages and applications. For instance, dual magnetrons with facing targets (where two cathodes, mostly consisting of the same material, are facing each other) are popular in depositing sensitive materials such as high-temperature superconductors [3, 4]. In this configuration, the substrate is placed outside this region to eliminate substrate bombardment with highly energetic species and substrate heating. Another configuration of a dual-magnetron setup consists of two single magnetrons that are mounted at 90° with respect to each other and each facing the substrate at 45° [5–9]. Such a configuration is often chosen to modify the stoichiometry of the complex oxide film in a flexible way. Indeed, by changing the target–substrate (T–S) distance and/or the target power for both cathodes independently, a large range of compositions can be

obtained [5, 6]. Willmott [10] considers the composition and growth control of complex metal oxides to be one of the future challenges for thin-film deposition. However, exact control of the independent dosing of individual metallic elements is still very problematic. Moreover, the stoichiometry of complex oxides strongly affects the properties of the films. Based on the above-mentioned considerations, we can say that there is a need to deeply investigate the behavior of the plasma species, as well as the deposition process, in a dual-magnetron sputter deposition system.

Reactive sputter deposition in a dual-magnetron discharge is studied by experiments and models; an overview of experimental and modeling studies can be found in [5, 6, 11]. These experiments enable us to study and explain relations between external parameters, such as cathode current and voltage, gas pressure, magnetic field, pumping speed and T–S distances, and measured properties, such as plasma species densities, fluxes and energies, erosion profiles, etc. However, some of these characteristics are difficult to measure due to possible plasma disturbance with the measuring tool (or limitations in size of the measuring tool). For this purpose, computer modeling can be very useful in calculating these plasma characteristics. On the other hand, the experiments remain unavoidable to validate the developed models. Moreover, certain input parameters are needed in models, which can be measured experimentally. Therefore, a combination of models and experiments is necessary to provide a complete chemical and physical picture of magnetron discharges.

Different modeling approaches exist to simulate magnetron discharges. Depending on the goal, the most relevant model can be chosen. In general, the models can be subdivided into analytical, continuum (or fluid) and particle models, as well as hybrid models, which can combine these model approaches. An analytical model is based on semi-empirical formulae describing the relation between certain plasma quantities and macroscopic parameters (e.g. voltage, current and pressure) [12, 13]. This model is very fast and can rapidly predict plasma behavior, but it is limited in accuracy (because of the approximations used) and valid for a limited range of conditions. In a fluid model [14], continuity equations of plasma species density, momentum and energy are solved, together with the Poisson equation to calculate the electric field distribution in a self-consistent way. This model is also fast and widely used to simulate gas discharges, when the plasma species are more or less in equilibrium with the electric field. However, in low-pressure discharges, such as magnetron discharges, the plasma species cannot be considered as a fluid, in equilibrium with the electric field. Moreover, the drift-diffusion approximation, which makes fluid models straightforward to implement, is invalid in magnetron discharges. On the other hand, so-called particle models are very suitable to simulate magnetron discharges. A particle-in-cell/Monte Carlo collisions (PIC/MCC) model [15–20] describes the behavior of the individual plasma particles (or superparticles (SPs)). Their trajectory in the electric and magnetic fields is calculated using Newton's laws, and their collisions are treated statistically, by random numbers. This model is very accurate, and moreover, it is self-consistent, i.e. it calculates the electric field in a self-consistent way. However, it requires a long calculation time, especially when modeling large and complicated reactor geometries, such as dual-magnetron configurations. A Monte Carlo (MC) model [21, 22] is similar to the PIC/MCC approach, because it also describes the trajectory of (super) particles by Newton's laws, and their collision by random numbers, but without solving the Poisson equation. Therefore, an MC model is not self-consistent and it requires a certain electric field distribution as input. Moreover, the so-called Bohm diffusion should be included explicitly in an MC model to account for time-dependent fluctuations in the electric field distribution [23].

On the other hand, it is much faster than the PIC/MCC approach, and therefore more suitable for large and complicated reactor geometries, such as dual-magnetron setups. Finally, a hybrid model [24], which combines different individual models, can be implemented to make use of the advantages and to avoid the limitations of the different models and also to achieve more reasonable computation times. However, such a hybrid model is usually based on the fluid approach, and therefore, it exhibits the same disadvantages as mentioned above for magnetron discharges.

Based on all these considerations, in this work we develop a so-called multi-species MC model [22], together with an analytical surface model [25] to describe the behavior of the important plasma species, as well as the deposition process of complex oxide thin films in a dual-magnetron discharge.

Our previous work was devoted to investigating electron behavior in a dual-magnetron discharge using an electron MC model [8]. With this model we were able to simulate the behavior of the fast electrons (i.e. the electrons with kinetic energies above the threshold for inelastic collisions). Their trajectory and their collisions with both background gas atoms and target atoms were described, and their densities and reaction rates were calculated. However, in order to obtain more insight into thin-film deposition of complex oxides, we need to also describe the other plasma species, such as Ar^+ ions, fast Ar atoms and sputtered metal atoms (i.e. Mg and Al atoms). Therefore, in this work we have extended the electron MC model to a multi-species MC model to describe the above-mentioned important plasma species. This multi-species MC model is based on the model of [22], but extended to a dual-magnetron setup. Moreover, we have combined this multi-species MC model to an analytical surface model (based on the model of [25]) to describe the deposition process of $Mg_xAl_yO_z$ thin films in a dual-magnetron discharge. Indeed, with this combined model we are able to predict both the plasma and surface properties for a broad variety of conditions in dual-magnetron setups, within a limited calculation time. The difference of this combined model with previous multi-species MC/analytical surface model is that (a) it can be used for large and geometrically complicated magnetron reactors (e.g. a dual-magnetron setup) and (b) the analytical surface model used in this work (see below) is much more complex than the analytical surface model used in [22] and it can be utilized to describe the deposition process of complex oxide films.

In our simulations, we have chosen the target (or cathode) materials as Mg and Al to investigate the deposition process of stoichiometric $Mg_xAl_yO_z$ thin films. The choice of these metals is based on the large amount of experimental data available, e.g. secondary electron emission coefficients (SEECs), sticking coefficients (SCs), sputter yields, etc (see e.g. [5, 25–27]). Moreover, many experimental and theoretical studies have been performed on magnesium aluminate 'spinel' ($MgAl_2O_4$) (see e.g. [28–32]). It is a unique material due to its optical, electrical, magnetic and mechanical properties and it is used as dielectric and irradiation resistant material in refractory ceramics [29]. It also has interesting catalytic properties (see e.g. [30, 31]) and can be applied as a covering material in high-pressure discharge lamps [32].

In this paper, some typical calculation results are presented, such as densities of the various plasma species, fluxes toward the targets and substrate and deposition rates. Moreover, the influence of the T–S distance on the deposition of the $Mg_xAl_yO_z$ films is also investigated.

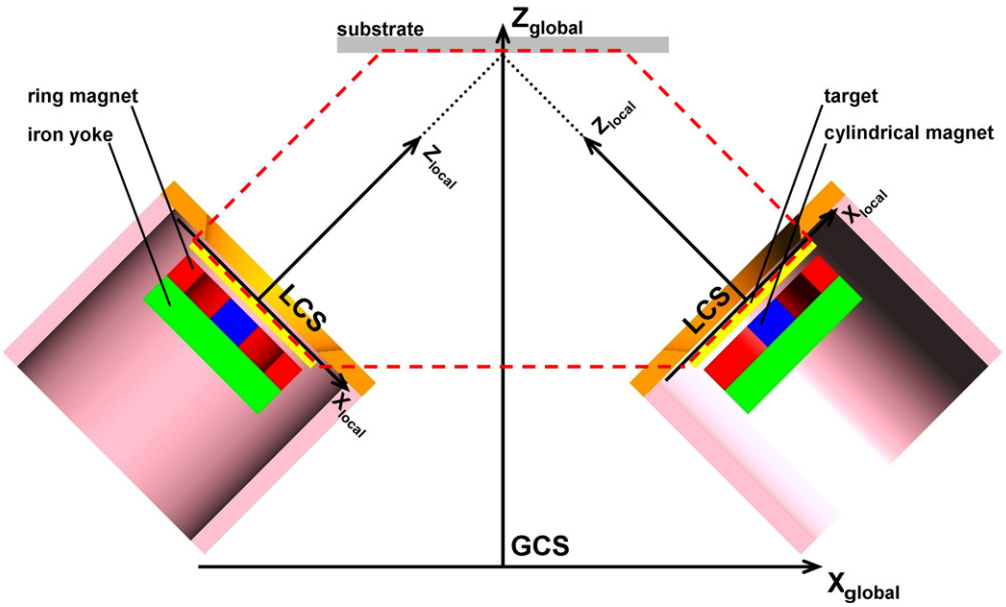

Figure 1. Schematic picture of the dual-magnetron configuration with the LCS and the GCS indicated. The T–S distance, i.e. the distance between the substrate (gray) center and the target (yellow) center is 10.5 cm. The boundary of the simulation area is presented by the dashed lines.

2. Description of the model

2.1. Multi-species Monte Carlo model

The presented multi-species MC model is three-dimensional (3D) in both the coordinate and the velocity space. For convenience, we need to use two different frames of reference in the dual-magnetron setup, i.e. a local coordinate system (LCS) of each magnetron source, and a global coordinate system (GCS). A schematic picture of the dual-magnetron setup, illustrating the LCS and the GCS, is presented in figure 1. The LCS of both magnetron sources is used to describe the trajectory and collision of the plasma species, but the resulting positions and velocities are also transferred to the GCS, so that the species are able to move from one magnetron source to the other (or in other words: from one LCS to the other).

A detailed overview of the multi-species MC model, albeit for a single magnetron discharge, can be found in [22]. In this paper, only a brief description is given. In the multi-species MC model, the real particles in the discharge are represented by a limited ensemble of SPs, with a certain weight corresponding to the number of real particles per SP. Only electrons, Ar^+ ions, fast Ar_f atoms and sputtered Mg and Al atoms are followed, because these species are considered to be important in the sputter deposition process. Indeed, the electrons are needed to create the Ar^+ ions. The fast Ar_f atoms are assumed to be formed by Ar^+ ions (i.e. by elastic collisions, i.e. isotropic and charge transfer, and by neutralization at the targets). Both Ar^+ ions and fast Ar_f atoms can sputter the Mg and Al targets. Note that the other plasma species, such as excited species and sputtered metal ions, are not included in this model, as they are considered to be of less importance [16]. Moreover, in this model, the metal atoms are sputtered from pure metallic targets, i.e. the flux of the reactive gas (in our case O_2) is only directed toward

the substrate and is high enough to obtain fully oxidized thin films but low enough to avoid target poisoning. This corresponds to the experimental conditions used to grow these $Mg_xAl_yO_z$ films [5, 11]. Therefore, because of the low density of reactive gas species in the bulk plasma, the collisions of these species with other plasma species in the reactor are not taken into account as well. The collisions of the species considered in the model (i.e. electrons, Ar^+ ions, fast Ar_f atoms and sputtered metal atoms), include elastic scattering, excitation to metastable and radiative states, ionization, charge transfer, etc and are presented in [22].

The MC models for electrons, Ar^+ ions, fast Ar_f atoms and sputtered Mg and Al atoms are run one after the other. The calculation starts with the fast electrons (see detailed description in [8]), which are emitted at both cathodes upon impact of the energetic plasma species (i.e. mainly Ar^+ and fast Ar_f). In this model, the initial number of the electron SPs emitted at the cathodes is 40 000. However, due to the ionization of the background gas atoms, these electrons can create secondary electrons, which are also followed in the model. Note that the number of secondary electrons can reach up to 12 times the number of primary electrons; so the total number of the electron SPs can be about 500 000. Based on the electron-impact ionization rate profile calculated in this electron MC model, the Ar^+ ions (or more specifically, the Ar^+ SPs) receive their initial positions and velocities, and are subsequently followed by the MC model for Ar^+ ions. Thereafter, the fast Ar_f atoms are followed; their initial positions and velocities are directly derived from the Ar^+ MC simulation. In principle, Ar^+ ions and fast Ar_f atoms can also create new electrons, by fast Ar^+ and Ar_f impact ionization [16], but the number of electrons created in this way is very low compared to the total number of electrons followed by the electron MC model (i.e. the ratio is less than 1%). Therefore, a coupling back from the Ar^+ and fast Ar_f MC models to the electron MC model was found to be unnecessary, in order not to complicate the simulations. As was mentioned before, both the Ar^+ ions and the fast Ar_f atoms sputter the Mg and Al targets, and as a consequence, the starting positions and velocities of the sputtered metal atoms are calculated from the fluxes of Ar^+ ions and fast Ar_f atoms toward the targets.

The electric and magnetic fields are given as input in the multi-species MC model. The electric field in each magnetron source was adopted from PIC/MCC simulations [16] and the magnetic field distribution in the entire dual-magnetron setup was calculated by using the open-source finite-element solver GetDP[4], together with the finite-element mesh generator Gmsh[5]. It should be mentioned that there are two possible magnetic field configurations in a dual-magnetron setup: a closed or a mirror configuration. A detailed description of the electric and magnetic field distributions and of the magnetic field configurations is given in our previous work [8]. Because of these configurations, a strong drift of the charged particles' guiding center can be observed. This drift is the result of a pronounced asymmetry of the discharge in a dual-magnetron setup (see [9]). In this work, we have considered closed magnetic field configuration. However, we expect that the choice of magnetic field configuration does not strongly influence the deposition of the sputtered metal atoms, based on the following.

1. The sputtered metal atoms are created at the targets (mostly by arriving Ar^+ ions, see below), where the magnetic field is symmetrically distributed (see the magnetic field distributions near the targets in [8]). Moreover, most energetic Ar^+ ions, which are responsible for sputtering of the metal atoms, are created near the targets: the electron

[4] http://www.geuz.org/getdp/
[5] http://www.geuz.org/gmsh/

impact ionization rate near the targets is almost 100 times higher than in the bulk area of the dual-magnetron setup (see [8]). It is also clear from [9] that the Ar^+ ions, which are created near the targets, are positioned symmetrically.

2. The sputtered metal atoms do not feel electric and magnetic fields, and as a consequence, an asymmetry of the discharge does not influence the deposition of these atoms on the substrate.

To verify these considerations, we have also performed calculations for the mirror magnetic field configuration to estimate the influence of the magnetic field configuration on the deposition of the metal atoms at the substrate and we have obtained the same results for both (closed and mirror) magnetic field configurations.

During consecutive time steps, the SPs' trajectory under the influence of both the electric and magnetic fields is calculated using Newton's equations of motion, based on the Lorentz force. This is true for the electron and Ar^+ ion SPs. The Ar_f and metal atom SPs of course do not feel the influence of the electric and magnetic fields. In the middle of each time step, the collisions are treated by a random number, which is uniformly distributed between 0 and 1. This random number is compared with the total collision probability (summed over all possible collision processes), which is calculated based on the collision cross sections (σ_k) or the reaction rate constants (k_k) and the target species densities (n_{tar}):

$$P_k = 1 - \exp(-\Delta t \cdot n_{\text{tar}} \cdot v \cdot \sigma_k(E_i)) \quad \text{or} \quad P_k = 1 - \exp\left(-\Delta t \cdot n_{\text{tar}} \cdot \frac{v}{\langle v \rangle} \cdot k_k(E_i)\right), \tag{1}$$

where P_k is the collision probability of kth type of collision, v is the velocity of the incident SP (and $\langle v \rangle$ is average velocity of SPs) and E_i is the energy of incident SP i. If the probability is lower than or equal to this random number, no collision occurs. If it is higher, a collision takes place. After the collision, the SP can be lost, or a secondary SP can be created (which is also followed in the calculation) or the SP can be scattered from its original path, after which it receives a new velocity (i.e. direction and magnitude). Details about the post-collision treatments for a magnetron discharge in argon are given in [15, 33, 34].

In a dual-magnetron setup, the plasma species can interact with the surfaces (i.e. the targets and the substrate), and can also cross the simulation area (the boundary of the simulation area is shown by dashed lines in figure 1). In our simulation, any particle reaching the boundary is considered to be lost eventually at the walls and will be removed from the simulation. The arriving particles to the surfaces can be adsorbed, reflected (as neutrals in the case of ions) or they can create new species [16, 22, 34]. More specifically, secondary electrons and/or sputtered atoms (i.e. Mg and Al) can be created. The yield of the secondary electrons is characterized by the SEEC. In this work, SEECs of Mg and Al targets are taken as 0.123 and 0.091, respectively [27]. The yield of sputtered atoms is determined by the Matsunami formula [35]. Reflection of electrons is treated by the reflection coefficient (RC = 0.1 [36]), whereas reflection of other particles is characterized by their SC. If the particle SC is zero, the particle is reflected when hitting the wall. On all surfaces, the SC is assumed to be zero for fast Ar_f atoms and Ar^+ ions, since Ar is an inert gas (note that Ar^+ ions are reflected as neutrals) [16], whereas the SC of both Mg and Al (and also for O_2 at the substrate, at least in the case of a pure metallic film) is proposed to be unity, i.e. they are stuck when bombarding the surface [37].

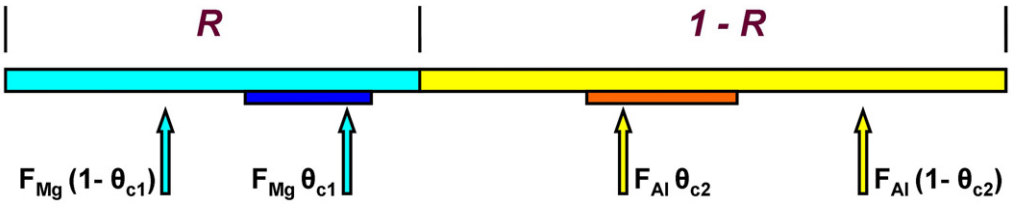

Figure 2. Schematic picture of the deposition process used in the analytical surface model. Sputtered metal fluxes arriving at the substrate are shown as blue (Mg) and yellow (Al) arrows. Note that the oxidized parts of the substrate are shown in darker blue (MgO) and orange colors (Al_2O_3). R is the Mg metal ratio ($R = N_{Mg}/(N_{Mg} + N_{Al})$).

2.2. Analytical surface model

As was mentioned above, an analytical surface model, i.e., the so-called Berg model [25], is coupled to our multi-species MC model to describe the deposition process of $Mg_xAl_yO_z$ thin films in a dual-magnetron discharge. The $Mg_xAl_yO_z$ system is used here as example, but of course the same methodology can be applied to other composite films as well. A more comprehensive description of the model is given by Berg and Nyberg [25] and the way for coupling this model to a plasma model can be found in [16, 22, 34]. However, in the present case, we deal with complex oxides, so the description is more complicated than in our previous studies [16, 22, 34]. Therefore, special attention is given here to the application of the model to the case of complex oxides in a dual-magnetron setup.

The analytical surface model for the deposition process from two separate targets is schematically presented in figure 2. Here, R is the so-called 'Mg metal ratio', i.e. the ratio between the number of Mg atoms arriving at the substrate and the total number of metal atoms (Mg and Al) on the substrate (i.e. $R = N_{Mg}/(N_{Mg} + N_{Al})$). We assume that all sputtered atoms (Mg and Al atoms, with certain SC) are uniformly deposited to the substrate. However, to explain the model, we subdivide for simplicity the substrate into two parts, i.e. an Mg and an Al part (see figure 2, blue and yellow areas). Since there is reactive gas (i.e. O_2 gas molecules; O atoms are not included in this model, as they were found to be negligible [16]) present near the substrate, the reaction between sputtered metal atoms and the reactive gas will cause a compound fraction θ_c of (one part of) the substrate to consist of compound molecules (see figure 2, darker blue and orange areas). θ_c is the ratio of the M_xO_y amount with desired stoichiometries (x and y), to the sum of the M_xO_y and the pure M amounts (here M stands for either Mg or Al). Note that the formation of the compound is of course again uniformly distributed over the whole substrate.

To describe the deposition process of the $Mg_xAl_yO_z$ film on the substrate, and to predict its stoichiometry, the effective sticking coefficients, S_{eff}, of O_2 need to be calculated. The values of S_{eff} depend on the already deposited amount of compound on the substrate, which is (as mentioned above) defined by the compound fraction, θ_c.

The general compound fraction balance equation for the deposition of O_2 (giving rise to two deposited O atoms) and M on the substrate to form an M_xO_y film with a desired stoichiometry (i.e. $x = 1$ and $y = 1$ in the case of MgO, and $x = 2$ and $y = 3$ in the case of

Al_2O_3) is:

$$\begin{aligned} 2F_{O_2}S_{O_2}(1-\theta_{c1}) &= F_{Mg}S_{Mg}\theta_{c1}, \\ 2F_{O_2}S_{O_2}(1-\theta_{c2}) &= \tfrac{3}{2}F_{Al}S_{Al}\theta_{c2}, \end{aligned} \tag{2}$$

where S_{O2}, S_{Mg} and S_{Al} are SCs of O_2, Mg and Al, respectively, and θ_{c1} and θ_{c2} stand for the Mg and Al compound fractions, respectively. Therefore, based on the fluxes (F) of the incoming species, together with the corresponding constant SC's of these species, the Mg and Al compound fractions on the substrate (on every grid cell) are calculated:

$$\begin{aligned} \theta_{c1} &= \frac{F_{O_2}S_{O_2}}{F_{O_2}S_{O_2} + \frac{1}{2}F_{Mg}S_{Mg}}, \\ \theta_{c2} &= \frac{F_{O_2}S_{O_2}}{F_{O_2}S_{O_2} + \frac{3}{4}F_{Al}S_{Al}}. \end{aligned} \tag{3}$$

Note that the fluxes of the sputtered Mg and Al atoms arriving at the substrate are calculated in the multi-species MC model. On the other hand, the flux of the O_2 molecules (F_{O2}) is assumed to be constant and uniformly distributed over the whole substrate area, and calculated according to the kinetic gas theory:

$$F_{O_2} = \frac{p_{O_2}v_{O_2}}{4k_BT}, \tag{4}$$

where p_{O2} is the O_2 gas pressure above the substrate, v_{O2} is the mean velocity of the O_2 gas molecules (defined from the gas temperature) and T is the background gas temperature.

As mentioned above, from the calculated compound fractions, the effective SC for the O_2 molecules, $S_{O2,eff}$, can now be calculated:

$$\begin{aligned} S^1_{O_2,\mathrm{eff}} &= S_{O_2}(1-\theta_{c1}), \\ S^2_{O_2,\mathrm{eff}} &= S_{O_2}(1-\theta_{c2}), \end{aligned} \tag{5}$$

where the superscripts 1 and 2 denote again the situation of the Mg and Al compounds, respectively. Note that a constant SC is used for Mg and Al (instead of S_{eff}) since they will stick equally well to a metallic surface and a surface covered with compound material.

With the effective sticking coefficients, the deposition rates of Mg, Al and O, i.e. D_{Mg}, D_{Al} and D_O, and also the total deposition rate, D_{tot}, can be found:

$$D_{Mg} = F_{Mg}S_{Mg}, \quad D_{Al} = F_{Al}S_{Al}, \tag{6}$$

$$D^1_O = 2F_{O_2}S^1_{O_2,\mathrm{eff}}R, \quad D^2_O = 2F_{O_2}S^2_{O_2,\mathrm{eff}}(1-R), \tag{7}$$

$$D_O = D^1_O + D^2_O, \quad D_{tot} = D_{Mg} + D_{Al} + D_O. \tag{8}$$

Finally, the stoichiometries of the deposited $Mg_xAl_yO_z$ film at steady state, x, y and z, are calculated by dividing the corresponding deposition rates by the total deposition rate, i.e.:

$$x = \frac{D_{Mg}}{D_{tot}}, \quad y = \frac{D_{Al}}{D_{tot}} \quad \text{and} \quad z = \frac{D_O}{D_{tot}}. \tag{9}$$

Note that in this work, the desired stoichiometric film is $MgAl_2O_4$, so that in order to find a lower index of the spinel (or magnesium aluminate), one should simply divide the stoichiometries x, y and z to x (see below in table 1).

Table 1. The stoichiometries x, y and z (and their ratio to x, blue color) of the deposited $Mg_xAl_yO_z$ films on the substrate, calculated with equation (9), for various T–S distances for both the Mg target (d_{Mg}) and the Al target (d_{Al}). The yellow-highlighted conditions correspond to a more or less stoichiometric $MgAl_2O_4$ film.

d_{Mg}	d_{Al}	Stoichiometry of Mg_x		Stoichiometry of Al_y		Stoichiometry of O_z	
(cm)	(cm)	x	x/x	y	y/x	z	z/x
10.5	18.5	0.389	1	0.037	0.095	0.574	1.472
10.5	16.5	0.387	1	0.057	0.148	0.555	1.433
10.5	14.5	0.382	1	0.083	0.216	0.535	1.402
10.5	12.5	0.362	1	0.13	0.358	0.508	1.404
10.5	10.5	0.337	1	0.198	0.586	0.465	1.379
12.5	10.5	0.238	1	0.256	1.076	0.506	2.126
14.5	10.5	0.144	1	0.297	2.068	0.559	3.883
16.5	10.5	0.094	1	0.306	3.277	0.6	6.417
18.5	10.5	0.067	1	0.307	4.609	0.626	9.377

3. Results and discussion

3.1. Operating conditions

The dual-magnetron device under study is a sputter deposition system with Mg and Al targets with a radius of 25 mm. It operates in a direct current mode, in Ar gas at 300 K and a gas pressure of 0.8 Pa. O_2 gas density in the bulk plasma is negligible, because the flux of O_2 gas is only directed to the substrate and is assumed uniformly distributed on it. Under these conditions, the targets remain in the metallic mode (i.e. not poisoned) and the substrate is fully oxidized. The discharge voltage is taken as −350 V and −450 V for the Mg and Al targets, respectively, and the discharge currents (I) are 0.5 A and 0.7 A for the Mg and Al targets, respectively. These are typical conditions used in experiments for growing $Mg_xAl_yO_z$ thin films by dual-magnetron sputtering [5, 11]. Note that in the experiments, the oxygen flow was regulated according to the T–S distances in order to achieve the desired stoichiometries, and to obtain fully oxidized films but no target poisoning, but the exact values were not mentioned explicitly (see [5, 11]). In our simulations, we use a constant value for the oxygen pressure, i.e. 0.32 Pa for all T–S distances. This value is used to calculate the O_2 gas flux (see equation (4)). This value is high enough to obtain the required stoichiometries, like in the experiments.

3.2. General plasma behavior

As mentioned above, in the multi-species MC model the calculations are performed for a theoretical number of SPs (per unit of time). However, the real values of the plasma species properties (such as densities and fluxes) need to be determined by multiplying the values of the calculated SP to the weight factor (W), which represents the total number of real particles per SP. The W can be obtained as follows, from the total number of electrons emitted per second at

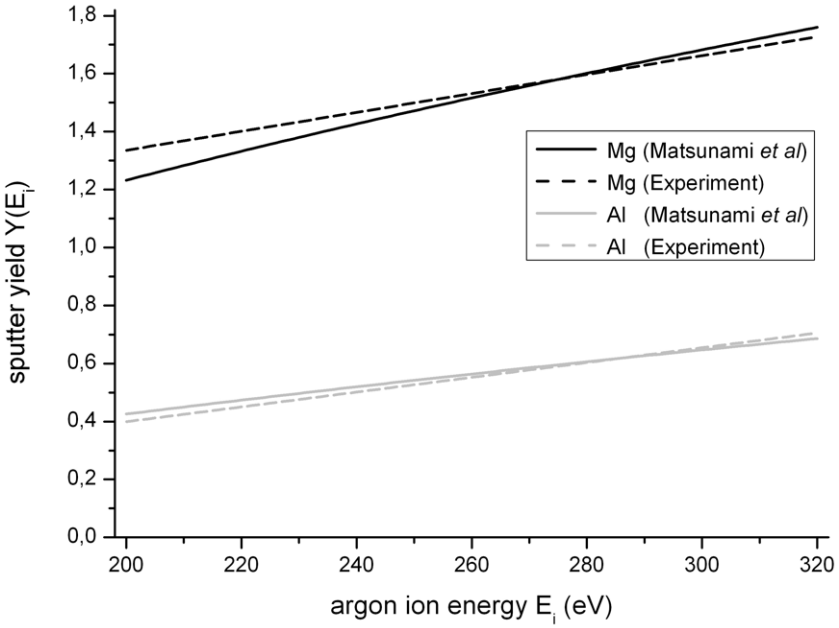

Figure 3. The sputter yields of Mg (black) and Al (gray) as a function of the incident Ar^+ ion energy, calculated with the Matsunami formula (solid lines) and determined by the experiment [5] (dashed lines).

both targets (i.e. the so-called real particles, RP_{e-}):

$$RP^1_{e-} = \frac{I_1}{q(1/\gamma_1 + 1)}, \quad RP^2_{e-} = \frac{I_2}{q(1/\gamma_2 + 1)}, \tag{10}$$

$$RP_{e-} = RP^1_{e-} + RP^2_{e-}, \quad W_{e-} = \frac{RP_{e-}}{SP_{e-}}, \tag{11}$$

where I_1 and I_2 (γ_1 and γ_2) are the cathode currents (and SEECs) of the Mg and Al targets, respectively, and q is the elementary charge. As soon as the weight factor for the electrons (W_{e-}) is determined, the same ratio applies for the Ar^+ ions, fast Ar_f atoms and sputtered (Mg and Al) atoms, because they are created (directly or indirectly) from the electrons (see above and see [22]). It should also be mentioned that in this work, the number of electrons starting at the cathodes is almost the same for the Mg and Al targets, i.e. 3.4×10^{17} and 3.6×10^{17} electrons are emitted per second from the Mg and Al targets, respectively (see equation (10), with $I_1 = 0.5$ A, $I_2 = 0.7$ A, $\gamma_1 = 0.123$ and $\gamma_2 = 0.091$; cf above).

As mentioned above, the creation of sputtered atoms is defined by the Matsunami formula [35]. However, in order to justify the calculated sputter yields by the Matsunami formula, we have compared them with the experimentally determined sputter yields [5]. Figure 3 illustrates that the calculated and experimental sputter yields correspond very well, at least in the Ar^+ ion energy range of interest in this work. For Mg, a slight deviation is observed, which is probably due to a strong influence of the surface binding energy and the unknown number of Ar atoms in the target during sputtering [38]. Note that the sputter yield of Mg is nearly three times greater than the sputter yield of Al, in the Ar^+ ion energy range of interest here.

The calculated 2D density profiles of the heavy species (i.e. Ar^+ ions, fast Ar_f atoms and sputtered Mg and Al atoms), are plotted in figure 4. The T–S distances (i.e. the distance between

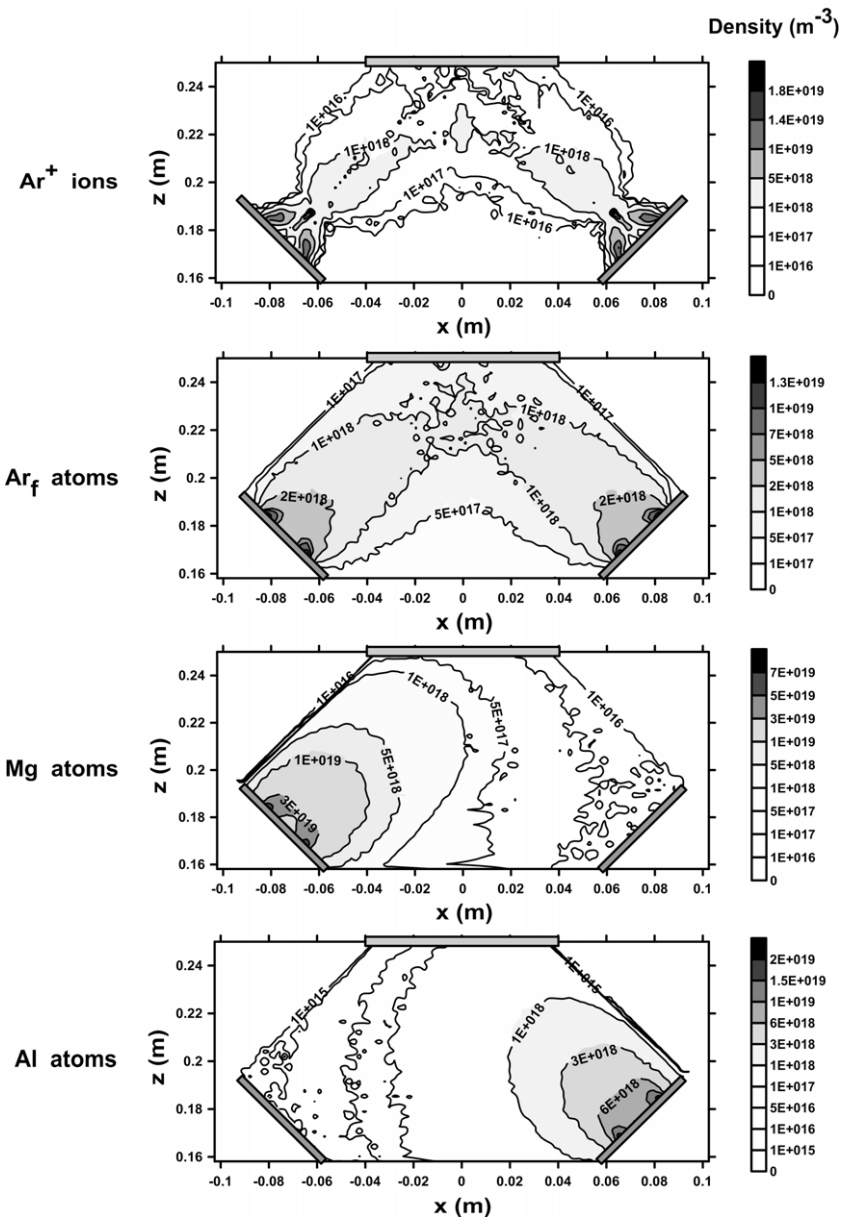

Figure 4. Calculated density profiles of the Ar^+ ions, fast Ar_f atoms and the sputtered Mg and Al atoms, in the dual-magnetron setup with the closed magnetic field configuration. The profiles are plotted in the *xz*-plane of the GCS (see figure 1). Both targets and substrate are indicated with gray rectangles. The T–S distances for both magnetrons are 10.5 cm.

the centers of the targets and the substrate) are taken to be the same, i.e. 10.5 cm, for both magnetrons. The electron density profile is not shown here, because it was already presented in [8], albeit for Ti targets, but we obtained a very similar profile in this study. Most of the plasma species are located near the targets. Indeed, due to the strong magnetic trap, the electron density, as well as the electron impact ionization rate, showed a maximum in this region [8], and the latter explains the maximum in the Ar^+ ion density. Moreover, as the fast Ar_f atoms

are created from the Ar^+ ions, it is logical that they also exhibit their maximum density in this region. Finally, the sputtered atoms are created at the targets, also explaining why their density reaches a maximum near the targets. The maxima of the Ar^+ ion density profiles are somewhat tilted toward the centers of both cathodes, which is caused by the similar tilted shape of the magnetic field (see magnetic field distributions in [8]), whereas in the case of the neutral species, i.e. the fast Ar_f atoms and the sputtered Mg and Al atoms, no tilted shape of the density profiles is apparent, because these species are not influenced by the electric and magnetic fields. It is obvious that the density of the Mg atoms reaches its maximum near the Mg target, but there are also some Mg atoms near the Al target. The same situation can be seen for the Al atoms. Moreover, the density of the Mg atoms is almost three times higher than the density of the Al atoms, which is explained by the three times higher sputter yield (note the different values in the color scales). It is also clear that the density profiles of the Ar^+ ions and the fast Ar_f atoms overlap in between the two magnetron regions due to the closed magnetic field configuration [8].

In figure 5, the profiles of the energy fluxes of the Ar^+ ions and the fast Ar_f atoms to the Mg target are presented, again at a T–S distance of 10.5 cm for both magnetrons. The corresponding energy fluxes to the Al target are the same, and are therefore not shown here. Indeed, as mentioned above, the number of electrons starting at both targets is almost the same and consequently the number of Ar^+ ions (created by the electrons, see above), as well as the number of fast Ar_f atoms (created by the Ar^+ ions) should be the same for both magnetrons. It is indeed clear from figure 4 that the maxima (and also the shapes) of the Ar^+ ion and fast Ar_f atom densities near both targets are the same. Note that the energy flux corresponds to the product of the species fluxes and their average energies, and hence, it is a measure of the amount of sputtering, as the flux defines the number of sputtering species and the energy determines the sputter yield. The energy fluxes of both the Ar^+ ions and fast Ar_f atoms reach their maximum at a radial position of about 12 mm, where the race track area is situated. It should be mentioned that although the number of incoming Ar^+ ions and fast Ar_f atoms to the targets is in the same order of magnitude (see the maxima of the densities of Ar^+ ions and fast Ar_f atoms, in figure 4), their average energies when bombarding the targets are not the same; the average energy of the Ar^+ ions is around 250 eV, whereas the average fast Ar_f atom energy is about 20 eV, i.e. approximately 13 times lower. This explains the lower energy flux of the fast Ar_f atoms compared to the Ar^+ ions. As a result, we can conclude that the Ar^+ ions will have a much higher contribution to the sputtering than the fast Ar_f atoms. Indeed, the relative contributions of Ar^+ ions and fast Ar_f atoms to the sputtering process were calculated to be about 96 and 4%, respectively.

Because the Ar^+ ion and fast Ar_f atom fluxes toward the targets show a peak profile at a radial position of around 12 mm, the sputtering of Mg and Al will also reach a maximum there, as is clear from figure 6, which illustrates the profiles of the total sputter fluxes of the Mg and Al atoms, again at a T–S distance of 10.5 cm for both magnetrons. The localized erosion creates the race track at a radial position of around 12 mm in the targets. As the sputter yield of Mg is almost three times higher than the Al sputter yield (cf figure 3 above), the Mg sputter flux is also about three times higher than the Al sputter flux, as is clear from figure 6. Therefore, we can already anticipate that in order to obtain the desired stoichiometric thin film (in our case $MgAl_2O_4$), one should increase the T–S distance for the magnetron with the Mg target or decrease the T–S distance for the magnetron with the Al target (see below).

Figure 7 presents the profiles of the Mg and Al fluxes toward the substrate holder, again at a T–S distance of 10.5 cm for both magnetrons. It is clear that the fluxes are not uniform over

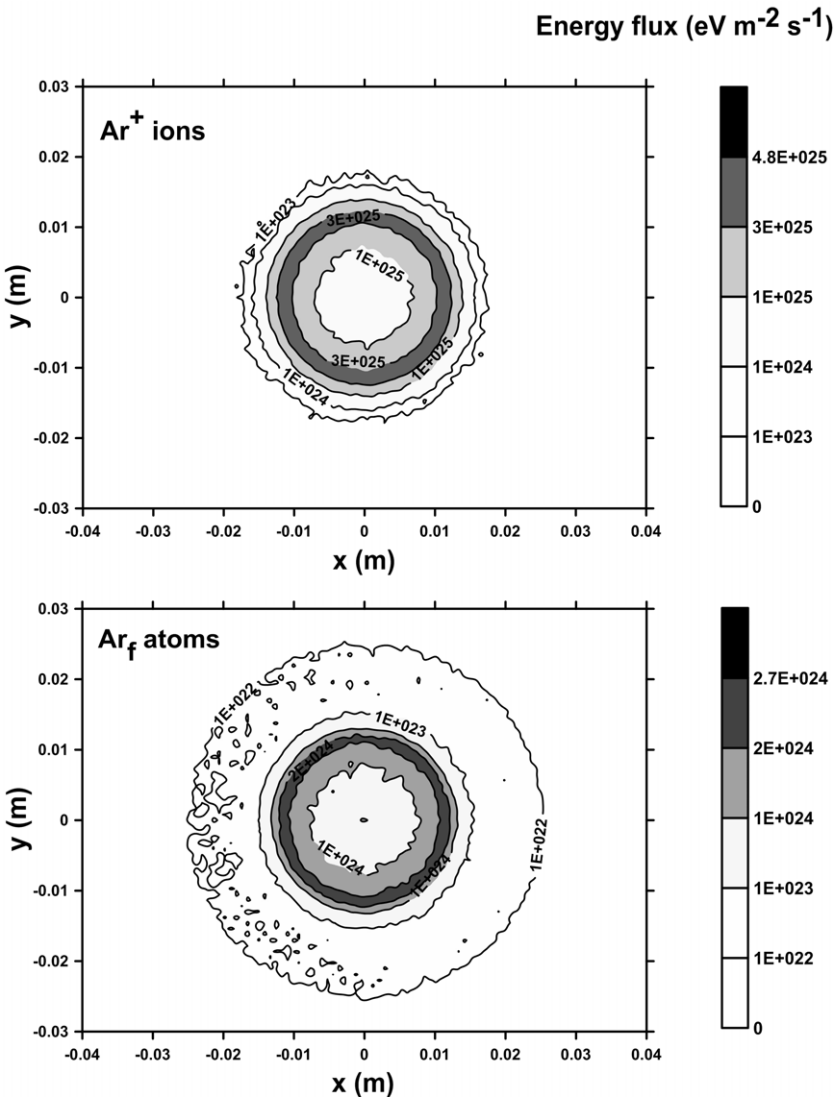

Figure 5. Calculated energy fluxes of the Ar^+ ions and fast Ar_f atoms to the Mg target. The profiles are plotted in the *xy*-plane of the LCS (see figure 1). The energy fluxes to the Al target are the same as to the Mg target, so they are not shown here.

the area of the substrate holder, indicating that the sputtered Mg and Al atoms are not deposited uniformly. Indeed, because of the alignment of the magnetrons the flux of Mg has its maximum at the left boundary of the substrate holder and vice versa, the flux of Al reaches its maximum value at the right boundary of the substrate holder. From the application point of view, the aim is of course to obtain a uniform film deposited on the substrate. Therefore, in the experiment the substrate was placed in the central area containing both Mg and Al atoms; see the small rectangle in figure 7, and the enlarged view in the figures at the right. The nonuniformity of the Mg and Al fluxes to the substrate is luckily far less pronounced than the nonuniformity of the fluxes to the entire substrate holder (cf the different scales of the color bars at the right).

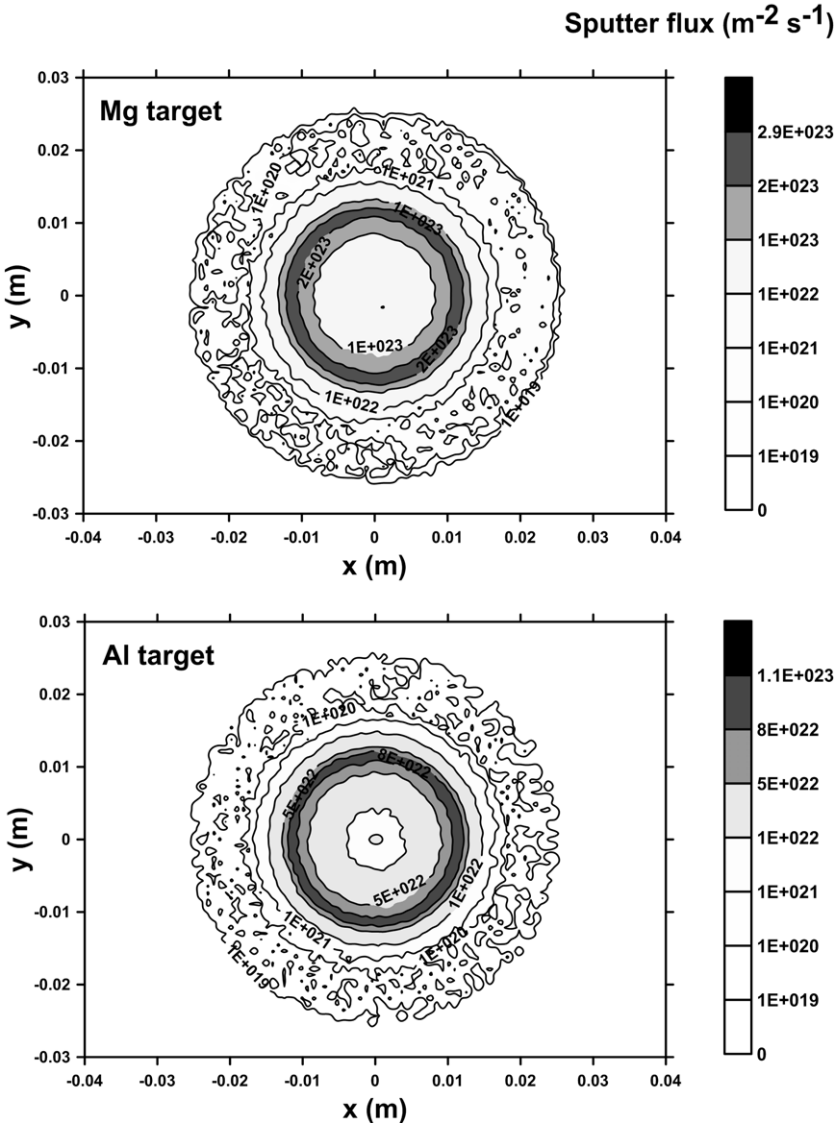

Figure 6. Calculated sputtered fluxes from the Mg and Al targets. The profiles are plotted in the *xy*-plane of the local coordinate systems (see figure 1). The localized erosion creates a race track (at a radial position of about 12 mm) in the targets.

Finally, based on these deposition fluxes, the film stoichiometry (at least, the Mg and Al metal ratios) can be estimated. It is clear from figure 7 that the Mg/Al ratio in this case is around 2, whereas for a stoichiometric spinel ($MgAl_2O_4$) film, the ratio would have to be 0.5. This indicates that the T–S distance of 10.5 cm for both magnetrons is not suited for obtaining a stoichiometric $MgAl_2O_4$ film, at least not for the discharge currents of 0.5 A and 0.7 A, used in this investigation. Therefore, in the following section, the effect of varying the T–S distance in both magnetron sources on the film stoichiometry will be investigated. It is clear that a similar study could be performed (and a similar effect can be obtained) by varying the discharge currents of both magnetrons.

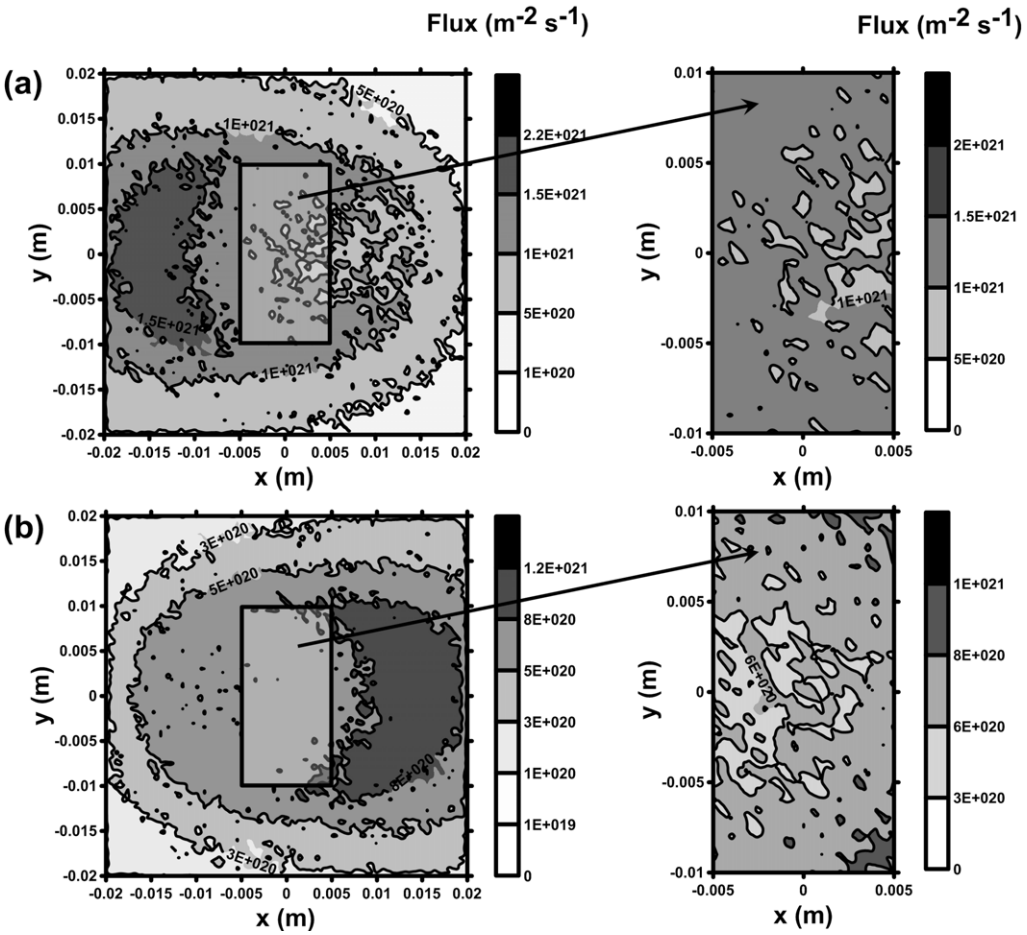

Figure 7. Calculated fluxes of the Mg (a) and Al (b) atoms toward the substrate. The profiles are plotted in the *xy*-plane of the GCS (see figure 1). The left-hand sides of the figures show the entire substrate holder. The small rectangles in these figures denote the substrate (grey color), for which the magnifications are shown on the right-hand sides of the figure.

3.3. Effect of target–substrate distance

The sputtered Mg and Al atoms from the two separate magnetrons move through the plasma and react with the oxygen gas molecules on the substrate to form complex oxide films (i.e. $Mg_xAl_yO_z$). It is obvious that the T–S distances of both magnetrons do affect the flux profiles of the Mg and Al atoms arriving at the substrate. In order to investigate the effect of T–S distance on the deposition process and to find a more suitable T–S distance for the desired stoichiometric thin film (i.e. $MgAl_2O_4$), two sets of simulations are performed. In the first set, the T–S distance for the magnetron with the Mg target (d_{Mg}) is kept constant at 10.5 cm, and the one for the magnetron with the Al target (d_{Al}) is varied between 10.5 and 18.5 cm (in steps of 2 cm). In the second set, the opposite is done: the T–S distance for the magnetron with the Al target is kept constant at 10.5 cm, and the one for the magnetron with the Mg target is varied between 10.5 and 18.5 cm.

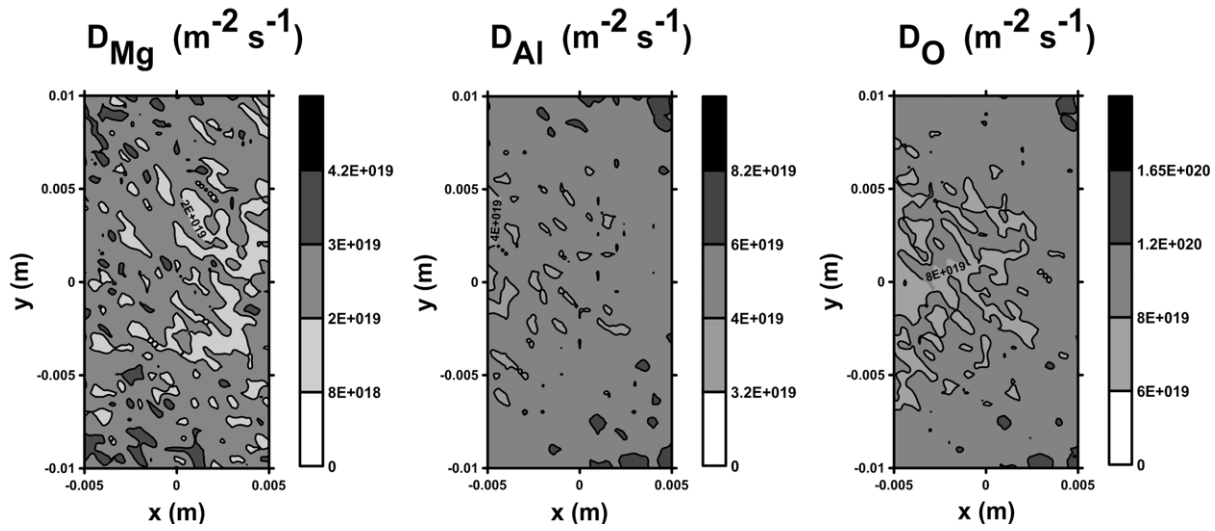

Figure 8. Calculated deposition rate profiles of the Mg, Al and O atoms at the substrate. The profiles are plotted in the *xy*-plane of the GCS (see figure 1). The T–S distances for the Mg and Al targets are 14.5 and 10.5 cm, respectively.

Table 1 illustrates the stoichiometries x, y and z of the deposited $Mg_xAl_yO_z$ film on the substrate, as well as their ratio to x (in blue), as calculated with equation (9). Note that the sum of x, y and z is equal to one, i.e. the sum of the deposition rates of Mg, Al and O is equal to the total deposition rate (see equations (8) and (9)). It is clear from table 1 that the most suitable T–S distance to obtain the desired stoichiometric film (i.e. $MgAl_2O_4$) is 14.5 cm for the magnetron with the Mg target and 10.5 cm for the magnetron with the Al target; indeed, this yields a film with stoichiometry $MgAl_{2.07}O_{3.88}$. A lower T–S distance for the Mg target and/or a higher T–S distance for the Al target give rise to a too low Al content, whereas a higher T–S distance for the Mg target and/or a lower T–S distance for the Al target would result in too much Al compared to Mg.

The calculated deposition rates of Mg, Al and O atoms are plotted over the entire surface area in figure 8, for the most suitable T–S distances, i.e. $d_{Mg} = 14.5$ cm and $d_{Al} = 10.5$ cm. It is clear that the deposition rate of Mg is now two times lower than the deposition rate of Al over the entire surface area of the substrate, whereas the deposition rate of oxygen atoms is approximately four (two) times higher than the deposition rate of Mg (Al) atoms. The deposition rates are slightly nonuniform, but this can also be partly due to statistics in the MC models.

To verify our model predictions, the Al metal ratios (i.e. $N_{Al}/(N_{Mg} + N_{Al})$), as calculated by the model, are compared with the experimental values, for the same Mg and Al T–S distances as used in the simulations, and the results are shown in figure 9. Note that in the experiment the Al metal ratio is calculated based on the determined chemical composition, which was obtained using an electron probe microanalyzer (EPMA) JEOL JXA-8621MX, with a beam current of 30 nA and a voltage of 15 keV (a detailed explanation is given in [5, 11]). It is clear from figure 9 that for a T–S distance of 14.5 cm for the Mg target, keeping the Al T–S distance fixed at 10.5 cm (see figure 9(a)), the Al metal ratio is almost twice as high as the Mg metal ratio in both the simulation and experiment (i.e. the simulations predict the Al metal ratio in this case to be ∼67%, whereas in the experiments a value of 61% is obtained). This confirms our predictions

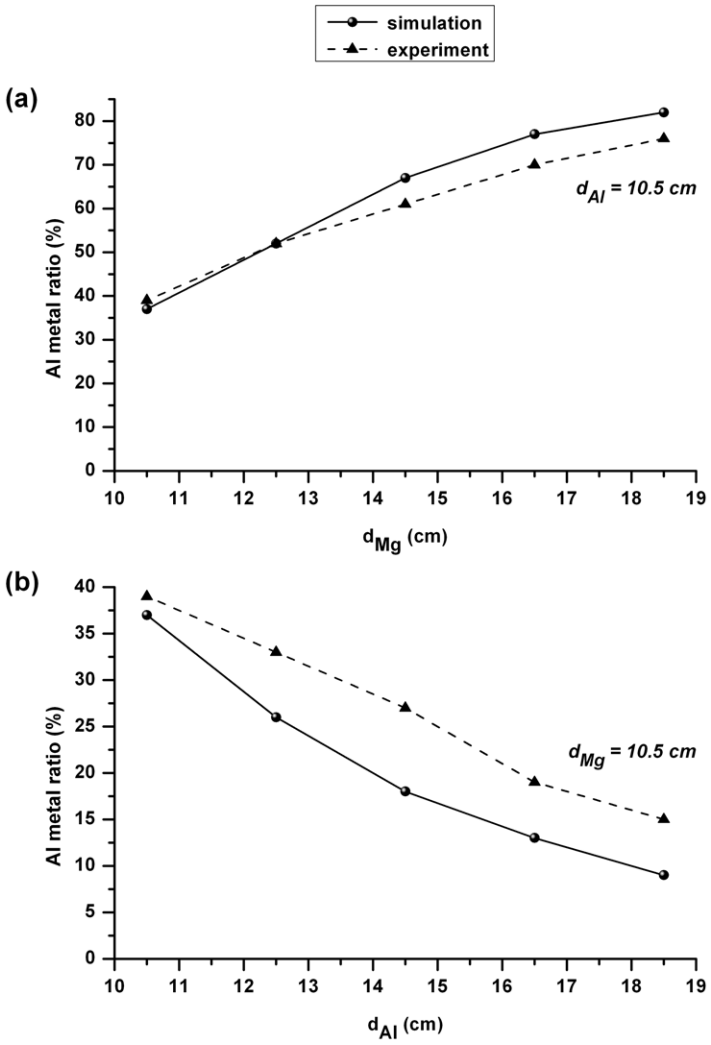

Figure 9. The Al metal ratio on the substrate predicted by the simulations and determined by the experiment, for different T–S distances. In (a) the T–S distance of the Mg target was varied, while keeping the T–S distance for the Al target constant, while in (b) the opposite was done, i.e. the Al T–S distance was varied for a fixed Mg T–S distance.

about the (more or less) stoichiometric film (i.e. $MgAl_2O_4$) under these conditions. In general, the results of both the simulations and experiments correspond well, for all T–S distances investigated, as is clear from figure 9. The slight differences between them can probably be attributed to the boundary of the simulation area (see above, section 2.1). Indeed, when the T–S distance is increased, the probability that a plasma species becomes lost (or more specifically, removed from the simulation) rises as well. Hence, if the T–S distance for the Mg target is increased, more Mg atoms will be lost and the Al metal ratio will be higher in the simulations, compared to the experimental values (see figure 9(a)). On the other hand, if the T–S distance for the Al target is increased, more Al atoms will be lost and therefore, the Al metal ratio obtained from the simulations will be lower than the experimental values (see figure 9(b)).

4. Conclusion

A combined multi-species MC/analytical surface model was developed for a dual-magnetron sputter-deposition device, to investigate the plasma behavior and the deposition process of $Mg_xAl_yO_z$ thin films. This is the first model, which is used for large and complicated magnetron reactor geometries, such as a dual-magnetron configuration.

With the multi-species MC model we are able to obtain a large variety of output data for the electrons, Ar^+ ions, fast Ar_f atoms and sputtered Mg and Al atoms, such as the densities, fluxes, average energies of the plasma species, as well as the collision rates. Typical results that are shown in this paper include the density profiles of the Ar^+ ions, fast Ar_f atoms and sputtered Mg and Al atoms, the fluxes of Ar^+ ions and fast Ar_f atoms toward the targets, and the fluxes of the sputtered Mg and Al atoms arriving at the substrate.

By combination of this multi-species MC model with an analytical surface model, we can also calculate the deposition rates of the sputtered metal and reactive gas atoms, as well as the film stoichiometry for various T–S distances, within a calculation time much shorter than in a PIC/MCC model (i.e. a factor of 20 shorter).

It was predicted that a T–S distance of 14.5 cm for the Mg target and 10.5 cm for the Al target gives rise to a more or less desired stoichiometric film (i.e. almost $MgAl_2O_4$). This calculation result was validated by comparison of the calculated Al metal ratio for different T–S distances with experimental data for the same conditions, and reasonable agreement was obtained.

Acknowledgments

This work was financially supported by the Fund for Scientific Research Flanders (FWO). The authors thank E Bultinck for her advice on the multi-species MC model and for the interesting discussions. This work was carried out using the Turing HPC infrastructure at the CalcUA core facility of the Universiteit Antwerpen, a division of the Flemish Supercomputer Center VSC, funded by the Hercules Foundation, the Flemish Government (department EWI) and the Universiteit Antwerpen.

References

[1] Depla D and Mahieu S 2008 *Reactive Sputter Deposition* (Berlin: Springer)
[2] Bradley J W, Thompson S and Gonzalvo Y A 2001 Measurement of the plasma potential in a magnetron discharge and the prediction of the electron drift speeds *Plasma Sources Sci. Technol.* **10** 490
[3] Imafuku M and Shimada H 1991 *In situ* epitaxial growth of YBCO films by facing targets sputtering method *Physica* C **185** 1967
[4] Zhao K, Zhou L Z, Leung C H, Yeung C F, Fung C K and Wong H K 2002 Epitaxial growth of oxide films (La–Ca–Mn–O and Y–Ba–Cu–O) by the facing-target sputtering technique *J. Cryst. Growth* **237** 608
[5] Saraiva M, Georgieva V, Mahieu S, Van Aeken K, Bogaerts A and Depla D 2010 Compositional effects on the growth of Mg(M)O films *J. Appl. Phys.* **107** 034902
[6] Georgieva V, Saraiva M, Jehanathan N, Lebelev O I, Depla D and Bogaerts A 2009 Sputter deposited Mg–Al–O thin films: linking molecular dynamics simulations to experiments *J. Phys. D: Appl. Phys.* **42** 065107
[7] Musil J and Baroch P 2005 Discharge in dual magnetron sputtering system *IEEE Trans. Plasma Sci.* **33** 338

[8] Yusupov M, Bultinck E, Depla D and Bogaerts A 2011 Behavior of electrons in a dual-magnetron sputter deposition system: a Monte Carlo model *New J. Phys.* **13** 033018
[9] Yusupov M, Bultinck E, Depla D and Bogaerts A 2011 Elucidating the asymmetric behavior of the discharge in a dual magnetron sputter deposition system *Appl. Phys. Lett.* **98** 131502
[10] Willmott P R 2004 Deposition of complex multielemental thin films *Prog. Surf. Sci.* **76** 163
[11] Saraiva M *et al* 2009 Influence of Al content on the properties of MgO grown by reactive magnetron sputtering *Plasma Process. Polym.* **6** S751
[12] Bradley J W, Arnell R D and Armour D G 1997 Measurement and modeling of the bulk plasma in magnetron sputtering sources *Surf. Coat. Technol.* **97** 538
[13] Buyle G, Depla D, Eufinger K, Haemers J, De Bosscher W and De Gryse G 2004 Simplified model for the dc planar magnetron discharge *Vacuum* **74** 353
[14] Costin C, Marques L, Popa G and Gousset G 2005 Two-dimensional fluid approach to the dc magnetron discharge *Plasma Sources Sci. Technol.* **14** 168
[15] Kolev I 2007 Particle-in-cell/Monte Carlo collisions simulations for a direct current planar magnetron discharge *PhD Thesis* University of Antwerp
[16] Bultinck E and Bogaerts A 2009 Particle-in-cell/Monte Carlo collisions treatment of an Ar/O_2 magnetron discharge used for the reactive sputter deposition of TiO_x films *New J. Phys.* **11** 103010
[17] Kolev I and Bogaerts A 2006 PIC-MCC numerical simulation of a dc planar magnetron *Plasma Process. Polym.* **3** 127
[18] Kolev I, Bogaerts A and Gijbels R 2005 Influence of electron recapture by the cathode upon the discharge characteristics in dc planar magnetrons *Phys. Rev.* E **72** 056402
[19] Kolev I and Bogaerts A 2008 Calculation of gas heating in a dc sputter magnetron *J. Appl. Phys.* **104** 093301
[20] Kolev I and Bogaerts A 2009 Numerical study of the sputtering in a dc magnetron *J. Vac. Sci. Technol.* A **27** 20
[21] Sheridan T E, Goeckner M J and Goree J 1990 Model of energetic electron transport in magnetron discharges *J. Vac. Sci. Technol.* A **8** 30
[22] Bultinck E and Bogaerts A 2011 Characterization of an Ar/O_2 magnetron plasma by a multi-species Monte Carlo model *Plasma Sources Sci. Technol.* **20** 045013
[23] Bultinck E, Mahieu S, Depla D and Bogaerts A 2010 The origin of Bohm diffusion, investigated by a comparison of different modelling methods *J. Phys. D: Appl. Phys.* **43** 292001
[24] Shidoji E, Ando E and Makabe T 2001 A comparative study of an unbalanced magnetron with dielectric substrate with a conventional magnetron through the use of hybrid modeling *Plasma Sources Sci. Technol.* **10** 621
[25] Berg S and Nyberg T 2005 Fundamental understanding and modeling of reactive sputtering processes *Thin Solid Films* **476** 215
[26] Depla D, Li X Y, Mahieu S and De Gryse R 2008 Determination of the effective electron emission yields of compound materials *J. Phys. D: Appl. Phys.* **41** 202003
[27] Depla D, Heirwegh S, Mahieu S, Haemers J and De Gryse R 2007 Understanding the discharge voltage behavior during reactive sputtering of oxides *J. Appl. Phys.* **101** 013301
[28] Bhaduri S and Bhaduri S B 2002 Microstructural and mechanical properties of nanocrystalline spinel and related composites *Ceram. Inter.* **28** 153
[29] Wdowik U D, Parlinski K and Siegel A 2006 Elastic properties and high-pressure behavior of $MgAl_2O_4$ from *ab initio* calculations *J. Phys. Chem. Solids* **67** 1477
[30] Di Cosimo J I, Diez V K, Xu M, Iglesia E and Apesteguia C R 1998 Structure and Surface and Catalytic Properties of Mg–Al Basic Oxides *J. Catal.* **178** 499
[31] Bocanegra S A, Ballarini A D, Scelza O A and De Miguel S R 2008 The influence of the synthesis routes of $MgAl_2O_4$ on its properties and behavior as support of dehydrogenation catalysts *Mater. Chem. Phys.* **111** 534
[32] Wei G C 2005 Transparent ceramic lamp envelope materials *J. Phys. D: Appl. Phys.* **38** 3057

[33] Kolev I and Bogaerts A 2006 Detailed numerical investigation of a dc sputter magnetron *IEEE Trans. Plasma Sci.* **34** 886

[34] Bultinck E 2009 Numerical simulation of a magnetron discharge utilized for the reactive sputter deposition of titanium nitride and oxide layers *PhD Thesis* University of Antwerp

[35] Matsunami N, Yamamura Y, Itikawa Y, Itoh N, Kazumata Y, Miyagawa S, Morita K, Shimizu R and Tawara H 1984 Energy dependence of the ion-induced sputtering yields of monoatomic solids *At. Data Nucl. Data Tables* **31** 1

[36] Bultinck E, Mahieu S, Depla D and Bogaerts A 2009 The reactive sputter deposition of a TiN film, simulated with a particle-in-cell/Monte Carlo collisions model *New J. Phys.* **11** 023039

[37] Van Aeken K, Mahieu S and Depla D 2008 The metal flux from a rotating cylindrical magnetron: a Monte Carlo simulation *J. Phys. D: Appl. Phys.* **41** 205307

[38] Mahieu S, Leroy W P, Depla D, Schreiber S and Moller W 2008 Noble gas retention in the target during rotating cylindrical magnetron sputtering *Appl. Phys. Lett.* **93** 061501